

Article

Effect of Surface Anions Adsorbed by Rutile TiO₂ (001) on Photocatalytic Nitrogen Reduction Reaction: A Density Functional Theory Calculation

Xiaoyu Jiang ^{1,†}, Mengyuan Gao ^{2,†} and Hongda Li ^{1,3,*} 

¹ Suzhou Institute for Advanced Research, University of Science and Technology of China, Suzhou 215123, China

² School of Materials Science and Engineering, Henan Normal University, Xinxiang 453007, China

³ School of Chemistry and Chemical Engineering, Hubei Normal University, Huangshi 435002, China

* Correspondence: hdli@ustc.edu.cn

† This author contributed equally to the work.

Abstract: The adsorption of common anions found in water can have a considerable impact on the surface state and optical characteristics of titanium dioxide (TiO₂), which has an important impact on the photocatalytic nitrogen reduction reaction (NRR). This work utilizes density functional theory (DFT) computations to examine the electronic and optical characteristics of the TiO₂ (001) surface under various anion adsorptions in order to clarify their influence on the photocatalytic NRR of TiO₂. The modifications in the structure, optical, and electronic properties of TiO₂ before and after anion adsorption are investigated. In addition, the routes of Gibbs free energy for the NRR are also evaluated. The results indicate that the adsorption of anions modifies the surface characteristics of TiO₂ to a certain degree, hence impacting the separating and recombining charge carriers by affecting the energy gap of TiO₂. More importantly, the adsorption of anions can increase the energy barriers for the NRR, thereby exerting a detrimental effect on its photocatalytic activity. These findings provide a valuable theoretical contribution to understanding the photocatalytic reaction process of TiO₂ and its potential application of NRR in the actual complex water phase.

Keywords: rutile TiO₂; nitrogen reduction reaction (NRR); DFT calculation; anion adsorption; photocatalysis



Citation: Jiang, X.; Gao, M.; Li, H. Effect of Surface Anions Adsorbed by Rutile TiO₂ (001) on Photocatalytic Nitrogen Reduction Reaction: A Density Functional Theory Calculation. *Molecules* **2024**, *29*, 4566. <https://doi.org/10.3390/molecules29194566>

Academic Editor: Adriana Dinescu

Received: 21 August 2024

Revised: 21 September 2024

Accepted: 24 September 2024

Published: 25 September 2024



Copyright: © 2024 by the authors. Licensee MDPI, Basel, Switzerland. This article is an open access article distributed under the terms and conditions of the Creative Commons Attribution (CC BY) license (<https://creativecommons.org/licenses/by/4.0/>).

1. Introduction

Due to constant population growth and the increasing tempo of industrialization, the problems concerned with energy and environmental deterioration have become more severe. Conventional resources of energy are scarce, and many of them are dwindling in their capacity to meet the growing demand [1]. Therefore, the challenge of constant energy consumption has led to research and development on renewable, clean, and efficient energy technologies. Photocatalysis, as one of the key approaches, has shown great promise in addressing energy limitations [2,3].

Of all the photocatalytic materials, TiO₂ stands out due to its favorable electronic structure; it can generate photo-induced electron–hole pairs under sunlight [4,5]. Due to its high chemical resistance and cheap price, it has become the object of research focus in the photocatalysis area [6]. Commercially, TiO₂ has been widely used in various photocatalytic reactions, includes hydrogen/oxygen production by water splitting [7,8], degradation of organic pollutants [9,10], CO₂ reduction [11], nitrogen reduction reaction (NRR) for ammonia synthesis, and so on [12]. Among them, the eco-friendly photocatalytic NRR is particularly prominent; it can convert N₂ into NH₃ at normal temperature and pressure, and the product, NH₃, is one of the key chemicals for maintaining the continuation of life on earth and meeting the needs of human society in the energy and chemical industries.

Rutile and anatase are two types of crystal phases of TiO_2 recognized for their superior electrical properties and photocatalytic efficiency [13]. Rutile TiO_2 is renowned for its exceptional chemical stability, particularly in demanding industrial settings characterized by high temperatures and severe pH levels [14]. Rutile TiO_2 has a wider bandgap; the material has a high photocatalytic activity mainly under UV light, and hence is ideal for photocatalytic processes that require effective separation of photogenerated electron–hole pairs [15]. A natural TiO_2 crystal predominantly exposes the (110), (111), and (001) facets. Among them, the (001) facet exhibits significantly higher normalized surface photo reactivity [16].

Photocatalytic processes with TiO_2 as the catalyst begin with the absorption of light. TiO_2 effectively produces electron–hole pairs when exposed to UV light. These pairs can then engage in redox processes [17]. The reactions mostly take place on the surface of TiO_2 , where the reactants are adsorbed and interact. The surface characteristics of TiO_2 play a crucial role in determining its total photocatalytic effectiveness [18,19]. Surface adsorption capacity, defect states, and surface charge distribution have a direct impact on the activation of reactants and the routes of reactions [20].

TiO_2 is extensively employed in aqueous photocatalytic reactions [21]. Nevertheless, real water environments consist of a multitude of anions, including fluoride (F^-), chloride (Cl^-), bromide (Br^-), iodide (I^-), sulfate (SO_4^{2-}), nitrate (NO_3^-), and carbonate (CO_3^{2-}) [22]. These anions readily adsorb onto the TiO_2 surface, potentially introducing surface states, altering the positions of the valence and conduction bands, and thereby affecting the bandgap. This in turn impacts the photocatalytic performance of TiO_2 [23]. Therefore, it is of great practical interest to examine the adsorption effects of these anions on the surface of TiO_2 and their impact on photocatalytic performance.

We conducted a comprehensive study on how the adsorption of common aqueous anions, including F^- , Cl^- , Br^- , I^- , NO_3^- , CO_3^{2-} , and SO_4^{2-} , affects the electrical and optical characteristics of the TiO_2 (001) surface. Using density functional theory (DFT) calculations, we analyzed changes in the bandgap, density of states (DOSs), optical absorption spectra, and Mulliken charge distribution before and after anion adsorption. Moreover, we examined the effects of anion adsorption on the Gibbs free energy of the NRR on TiO_2 . This proves that anion adsorption does indeed affect the photocatalytic behavior of TiO_2 in a negative manner. These findings not only provide a significant theoretical framework and guidance for using TiO_2 photocatalysts in multicomponent aqueous systems, but are also applicable to electrocatalytic nitrogen fixation, further expanding its potential applications in clean energy technologies [24,25].

2. Results and Discussion

2.1. Adsorption Models and Adsorption Energies

As shown in Figures 1 and 2, the study focuses on the adsorption of halide anions on two specific spots of the rutile TiO_2 (001) surface, namely, directly above the O atom and directly above the Ti atom. These sites are denoted as $\text{TiO}_2\text{-O-X}^-$ and $\text{TiO}_2\text{-Ti-X}^-$ ($\text{X} = \text{F}, \text{Cl}, \text{Br}, \text{I}$), respectively. For the adsorption of NO_3^- , CO_3^{2-} , and SO_4^{2-} anions, only the adsorption site directly above the Ti atom was considered, denoted as $\text{TiO}_2\text{-NO}_3^-$, $\text{TiO}_2\text{-CO}_3^{2-}$, and $\text{TiO}_2\text{-SO}_4^{2-}$, respectively.

Table 1 provides a thorough examination of the changes in bond length and adsorption energy on the rutile TiO_2 (001) surface when different anions are adsorbed. We labeled the four edges surrounding the Ti atom beneath the adsorbed ion as a, b, c, and d, and measured the average lengths of these edges for the eight Ti–O bonds directly below. The results show that the adsorption of all anions causes an elongation of these O–Ti bonds. Among the halide anions adsorbed at the Ti site (F^- , Cl^- , Br^- , I^-), F^- induces the most significant bond elongation, with the bond length reaching 1.950 Å. This is complemented by the most negative adsorption energy of -3.505 eV. As the atomic radius of the halogen increases from Cl^- to I^- , both the adsorption energy and the extent of bond elongation decrease accordingly. When comparing the adsorption of halide anions at the Ti and O

sites, it is discovered that adsorption at the O site leads to a somewhat lower elongation of the O-Ti bond compared to the Ti site. Likewise, the adsorption energies at the O site regularly exhibit less negative values compared to those at the Ti site. Therefore, all the following computations were conducted with the Ti site.

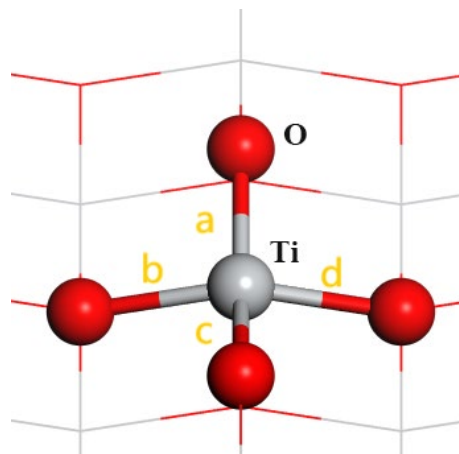


Figure 1. Model of the rutile TiO_2 (001) surface. The four Ti-O bonds connected by Ti atoms below the adsorbed ion are a, b, c and d; Gray ball is Ti atom, red balls are O atom.

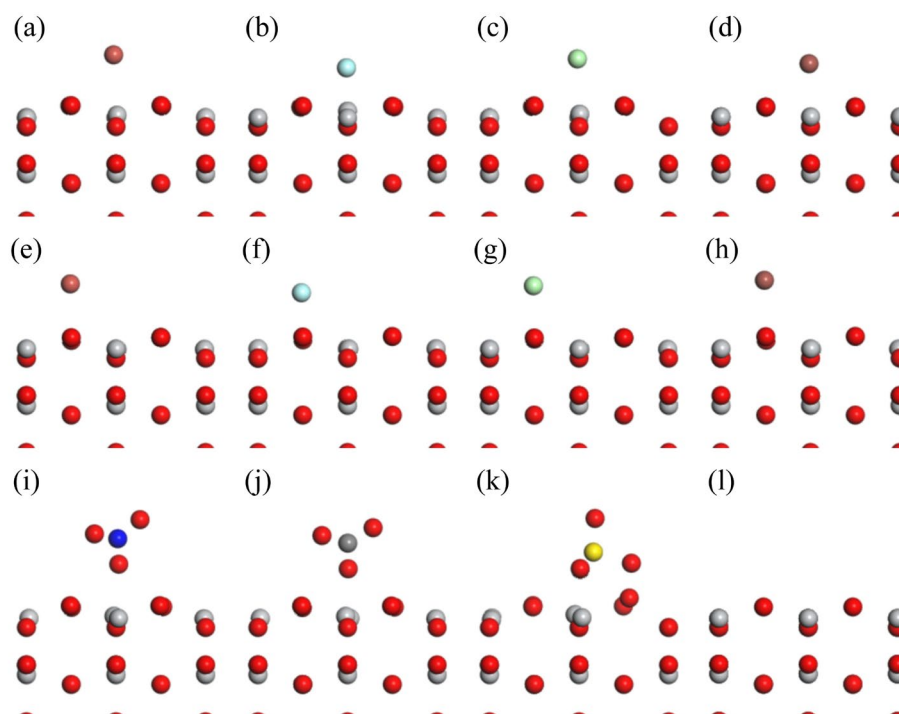


Figure 2. The models before and after anion adsorption: (a–l) represent $\text{TiO}_2\text{-Ti-F}^-$, $\text{TiO}_2\text{-Ti-Cl}^-$, $\text{TiO}_2\text{-Ti-Br}^-$, $\text{TiO}_2\text{-Ti-I}^-$, $\text{TiO}_2\text{-O-F}^-$, $\text{TiO}_2\text{-O-Cl}^-$, $\text{TiO}_2\text{-O-Br}^-$, $\text{TiO}_2\text{-O-I}^-$, $\text{TiO}_2\text{-NO}_3^-$, $\text{TiO}_2\text{-CO}_3^{2-}$, $\text{TiO}_2\text{-SO}_4^{2-}$, and TiO_2 , respectively.

Besides halide anions, the study of complex anion adsorption (NO_3^- , CO_3^{2-} , SO_4^{2-}) on the surface structure of TiO_2 is also examined in this work. It is found that all three anions lead to good chemisorption, with the SO_4^{2-} anion having the highest effect because of its large multi-atomic anion. This includes an adsorption energy of -3.025 eV and the largest degree of bond extension by 1.950 Å. These facts show that the interaction of complex anions in the solution with the TiO_2 surface may lead to impressive distortions of the crystal lattice.

Table 1. Comparison of Ti-O bond length and E_{ads} before and after anion adsorption for rutile TiO₂ (001).

Configurations	Average Ti-O Bond Length (Å)	E_{ads} (eV)
TiO ₂ (001)	1.936	/
TiO ₂ -Ti-F ⁻	1.950	-3.505
TiO ₂ -Ti-Cl ⁻	1.948	-0.913
TiO ₂ -Ti-Br ⁻	1.946	-1.075
TiO ₂ -Ti-I ⁻	1.944	-1.504
TiO ₂ -O-F ⁻	1.942	-1.545
TiO ₂ -O-Cl ⁻	1.940	-0.812
TiO ₂ -O-Br ⁻	1.938	-0.631
TiO ₂ -O-I ⁻	1.937	-0.603
TiO ₂ -NO ₃ ⁻	1.945	-0.896
TiO ₂ -CO ₃ ²⁻	1.947	-1.278
TiO ₂ -SO ₄ ²⁻	1.950	-3.025

2.2. Electronic Structure

The changes in the band structure are of critical importance to the photocatalytic activity of TiO₂ as they determine the material's optical response range and electron transport characteristics [26]. In general, a narrower bandgap enables the material to capture a wider variety of light wavelengths, which in turn increases its ability to catalyze chemical reactions when exposed to visible light [27]. Nonetheless, a desirable bandgap is when it is not too small since it may lead to early recombination of electron-hole pairs, thus reducing the photocatalysis effect [28]. In this study, we calculated the interfacial bandgap and band alignments of TiO₂ before and after anion adsorption, as illustrated in Figures 3 and 4, respectively. The pristine rutile TiO₂ (001) surface exhibits a bandgap of 2.45 eV. Significant alterations in the bandgap were detected with the adsorption of anions. For halide anions adsorbed at the Ti site, the bandgaps of the TiO₂-Ti-F⁻, TiO₂-Ti-Cl⁻, and TiO₂-Ti-Br⁻ systems increased to 3.39 eV, 3.23 eV, and 3.14 eV, respectively, indicating a widening of the bandgap, with fluorine having the most pronounced effect. In contrast, the TiO₂-Ti-I⁻ system, following I⁻ adsorption, likely formed localized states, leading to a substantial reduction in the bandgap to 1.59 eV.

The bandgaps of the TiO₂-NO₃⁻, TiO₂-CO₃²⁻, and TiO₂-SO₄²⁻ systems were calculated to be 3.27 eV, 3.29 eV, and 2.40 eV, respectively, for the adsorption of complex anions. The substantial increase in bandgap resulting from the adsorption of NO₃⁻ and CO₃²⁻ indicates a robust electrical interaction with the surface of TiO₂. In contrast, the little reduction in the bandgap after the adsorption of SO₄²⁻ might be ascribed to the bulky molecular structure of the sulfate ion, which could lead to electronic rearrangement on the surface.

The density of states (DOSs) analysis is a powerful tool for elucidating the distribution of electrons across various energy levels and for identifying the contributions of specific atoms and orbitals to the overall electronic structure. In Figure 5, the DOSs of the TiO₂ show that the valence band (VB) is mainly composed of the oxygen 2p orbitals, while the conduction band (CB) is mainly composed of titanium 3d orbitals. The analysis of the electronic structure of TiO₂ revealed that the adsorption of NO₃⁻, CO₃²⁻, and SO₄²⁻ organic anions has a weak impact on the material. This suggests that the N, C, and S orbitals of these complex anions have a negligible impact on the valence and conduction bands of TiO₂.

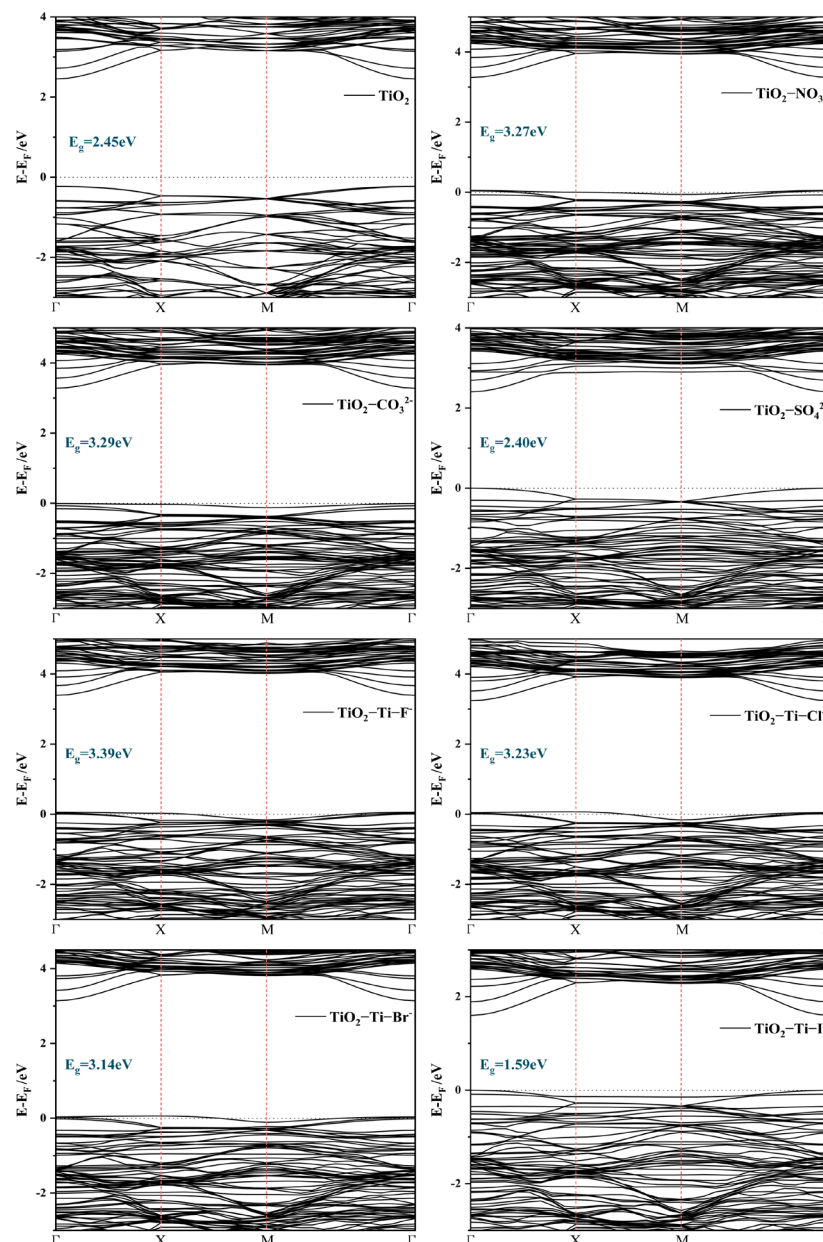


Figure 3. The band structures of TiO_2 , $\text{TiO}_2\text{-NO}_3^-$, $\text{TiO}_2\text{-CO}_3^{2-}$, $\text{TiO}_2\text{-SO}_4^{2-}$, $\text{TiO}_2\text{-Ti-F}^-$, $\text{TiO}_2\text{-Ti-Cl}^-$, $\text{TiO}_2\text{-Ti-Br}^-$, and $\text{TiO}_2\text{-Ti-I}^-$. The red dotted line represents high symmetry points.

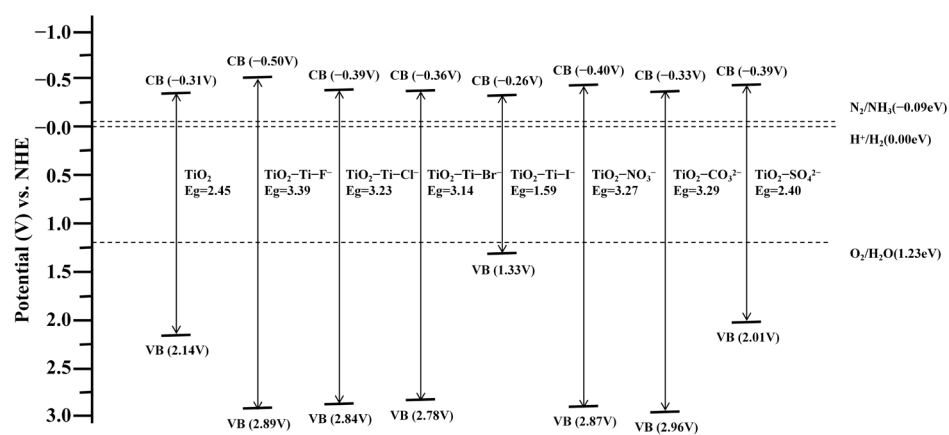


Figure 4. The band alignments before and after anion adsorption.

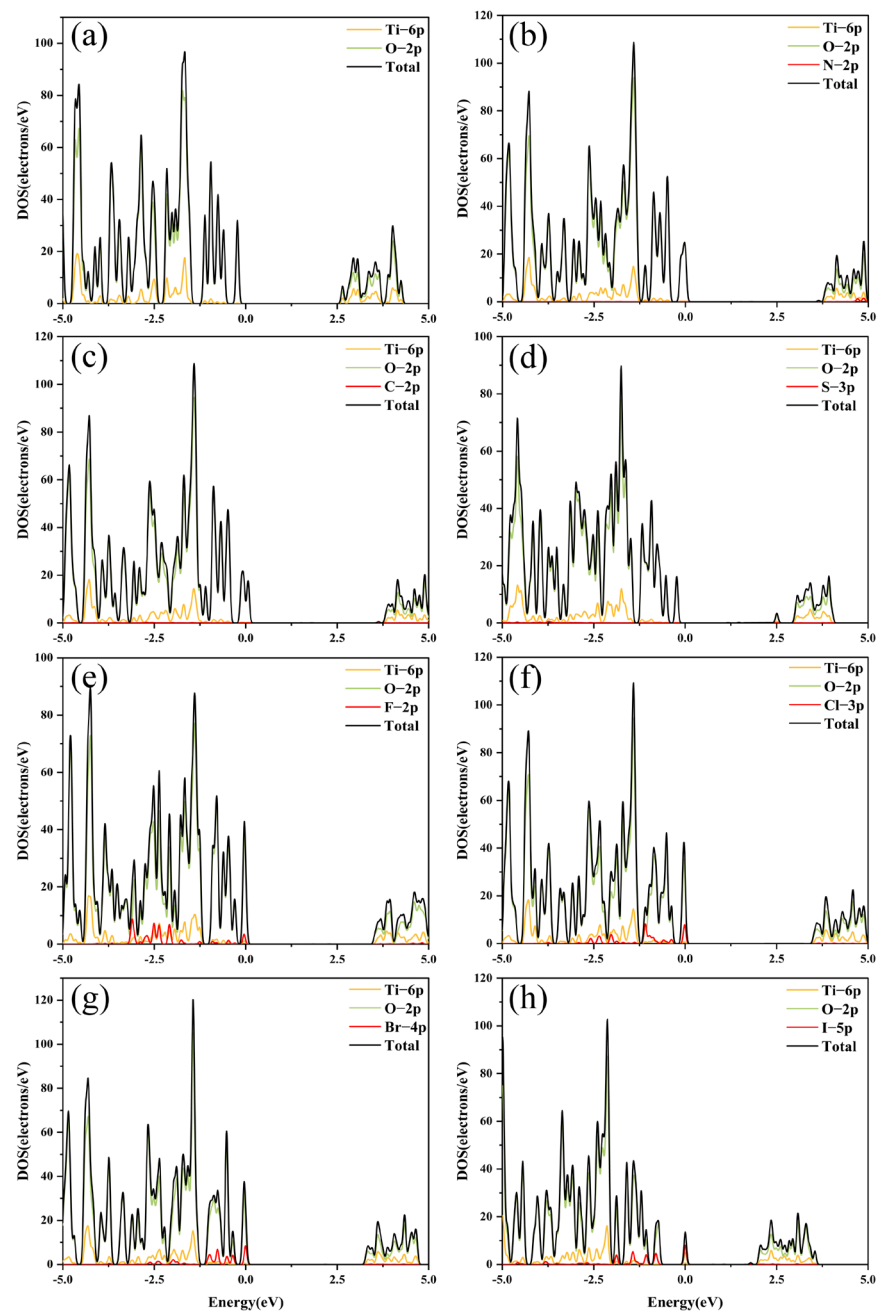


Figure 5. (a–h) Density of states of TiO_2 , $\text{TiO}_2\text{-NO}_3^-$, $\text{TiO}_2\text{-CO}_3^{2-}$, $\text{TiO}_2\text{-SO}_4^{2-}$, $\text{TiO}_2\text{-Ti-F}^-$, $\text{TiO}_2\text{-Ti-Cl}^-$, $\text{TiO}_2\text{-Ti-Br}^-$, and $\text{TiO}_2\text{-Ti-I}^-$.

Nevertheless, a noticeable change in the electronic configuration is noticed when halogen anions are adsorbed into the surface of TiO_2 . The outer orbitals of the halogen atoms not only contribute to the modification of the valence band but also lead to the formation of localized states, particularly in the case of I^- . The emergence of these localized states around the Fermi level leads to a substantial decrease in the band gap of TiO_2 . In contrast, the adsorption of F^- and Cl^- induces a relatively broad energy dispersion, whereas Br^- exhibits the most pronounced energy localization. This localization may give rise to deep-level defect states, potentially impacting the photoelectric properties of the material.

The Mulliken charge analysis data, as shown in Table 2, provide a detailed view of the electron transfer dynamics within the TiO_2 (001) surface following the adsorption of various complex anions. Among the complex anions studied, the $\text{TiO}_2\text{-NO}_3^-$ complex

exhibits the most pronounced electron transfer, indicating a strong interaction between the NO_3^- anion and the TiO_2 surface. This is followed by $\text{TiO}_2\text{-CO}_3^{2-}$ and $\text{TiO}_2\text{-SO}_4^{2-}$, both of which also show significant, albeit varying, degrees of electron transfer.

Table 2. The Mulliken charges before and after adsorption.

Configurations	Mulliken Charge (e)
TiO_2 (001)	2.49
$\text{TiO}_2\text{-Ti-F}^-$	2.28
$\text{TiO}_2\text{-Ti-Cl}^-$	2.32
$\text{TiO}_2\text{-Ti-Br}^-$	2.36
$\text{TiO}_2\text{-Ti-I}^-$	2.24
$\text{TiO}_2\text{-NO}_3^-$	2.30
$\text{TiO}_2\text{-CO}_3^{2-}$	2.34
$\text{TiO}_2\text{-SO}_4^{2-}$	2.37

In systems involving halogen anion adsorption, the $\text{TiO}_2\text{-Ti-I}^-$ complex demonstrates the highest level of electron transfer, followed by $\text{TiO}_2\text{-Ti-F}^-$, $\text{TiO}_2\text{-Ti-Cl}^-$, and $\text{TiO}_2\text{-Ti-Br}^-$. The adsorption of all these anions results in a redistribution of electrons across the TiO_2 surface.

After adsorption, the electron density is mostly concentrated around the adsorbed anions, resulting in a decrease in electron density on the TiO_2 (001) surface. This redistribution of electrons alters the electronic environment of the TiO_2 surface, thereby modifying its surface properties and potentially influencing its catalytic behavior.

2.3. Optical Absorption

The optical absorption spectrum can be obtained through linear response theory. First, the real and imaginary parts of the dielectric function ($\epsilon(\omega)$) are calculated, and then the optical absorption spectrum is derived by analyzing the imaginary part of the dielectric function ($\text{Im } \epsilon(\omega)$).

The UV-Vis absorption spectra of TiO_2 samples before and after anion adsorption were measured, as depicted in Figure 6. It is evident that anion adsorption significantly alters the optical properties of TiO_2 . The pristine TiO_2 sample exhibits a strong absorption peak around 480 nm. However, following anion adsorption, the samples display varying degrees of peak shifts and changes in absorption intensity.

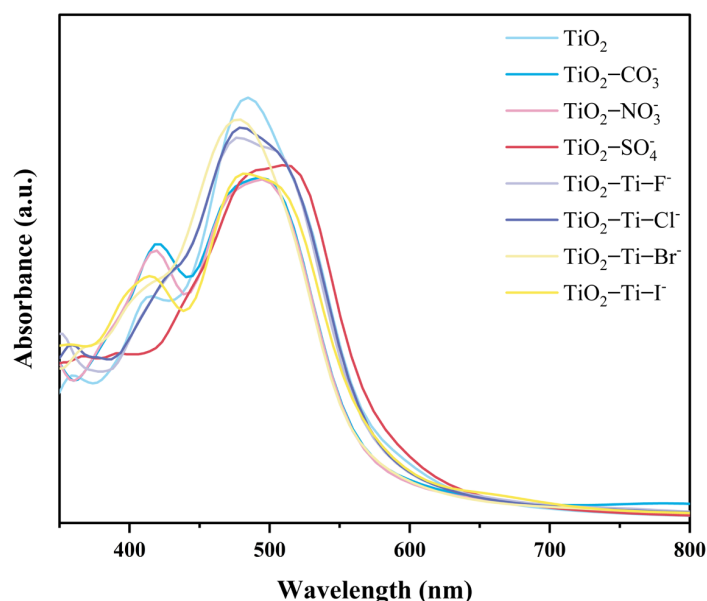


Figure 6. The optical absorption spectra before and after anion adsorption.

For TiO₂ adsorbing NO₃[−], CO₃^{2−}, and SO₄^{2−}, while the primary absorption characteristics remain similar to those of pristine TiO₂, the intensity changes are more pronounced, particularly with a noticeable decrease in the absorption intensity near 480 nm. On the other hand, the adsorption of halide anions (F[−], Cl[−], Br[−], and I[−]) leads to significant red shifts and blue shifts in the TiO₂ absorption peaks. The absorption intensity is notably higher compared to the samples adsorbing NO₃[−], CO₃^{2−}, and SO₄^{2−}. Specifically, the adsorption of F[−] and Cl[−] results in a marked red-shift of the TiO₂ absorption peak, extending the absorption range to longer wavelengths. In comparison, the adsorption of Br[−] and I[−] causes smaller peak shifts but still affects the absorption characteristics.

Overall, the adsorption of anions induces substantial modifications in the optical absorption properties of TiO₂, particularly affecting its visible light absorption characteristics.

2.4. NRR Gibbs Free Energy Pathway

The nitrogen reduction reaction (NRR) shows great potential in the fields of environmental protection and energy production, particularly in the realms of sustainable agriculture and green chemistry [29]. The synthesis of ammonia (NH₃) is a critical process in modern industry, serving as a key intermediate in fertilizer production and, potentially, as a hydrogen carrier in the future, offering a clean and efficient energy solution. The nitrogen molecule (N₂) is characterized by an exceptionally high bond dissociation energy (approximately 941 kJ/mol) and the extraordinary stability of the N≡N triple bond [30]. Therefore, a catalyst capable of effectively activating and reducing N₂ must possess robust electron transfer capabilities and stable reactive sites. These sites need to effectively adsorb and activate N₂ molecules, as well as support the consecutive electron transfer and hydrogenation processes necessary for the reduction of N₂ to NH₃. Therefore, it is necessary to have catalyst materials with outstanding surface electronic properties that can be consistently maintained to facilitate uninterrupted photocatalytic reactions. TiO₂ with its efficient charge separation capabilities and chemical stability, has emerged as a focal point in photocatalytic NRR research [31]. Anions present in water include F[−], Cl[−], Br[−], I[−], NO₃[−], CO₃^{2−}, and SO₄^{2−} adsorb on the surface of TiO₂ and modify the electronic structure, and therefore, the activity of the catalyst in NRR. Consequently, among the various photocatalytic reactions, we have prioritized NRR for evaluating catalyst efficiency. Investigating the catalytic performance of TiO₂ before and after anion adsorption will be useful for the improvement of TiO₂-based NRR catalysts.

The photocatalytic NRR commonly follows the alternating hydrogenation mechanism as the predominant reaction pathway [32,33]. In order to investigate the impact of anion adsorption on the photocatalytic performance of TiO₂, we examined the changes in Gibbs free energy for all materials involved in this process, as depicted in Figure 7. The initial hydrogenation step (Equation (2)) within the alternating hydrogenation mechanism, which marks the onset of the NRR process, is recognized as the rate-determining step, meaning it determines the entire reaction rate and acts as a bottleneck [34].

Our observations indicate that the Gibbs free energy change for the initial hydrogenation step on pure TiO₂ remains relatively small, both before and after anion adsorption. The impact of anion adsorption on the TiO₂ catalyst varies significantly depending on the type of anion. The Gibbs free energy change for the rate-determining step on pure TiO₂ is 1.81 eV; for polyatomic anions such as NO₃[−], CO₃^{2−}, and SO₄^{2−}, the ΔG increases to 2.35 eV, 2.4 eV, and 2.25 eV, respectively, which is notably higher than the 1.81 eV of pure TiO₂. The notable impact may be ascribed to the intricate molecular compositions of these substances, which cause substantial deformation of the crystal structure and reorganization of the electrical configuration on the surface of TiO₂. In contrast, the impact of monoatomic anions is relatively moderate. For instance, the ΔG after I[−] adsorption is 2.16 eV, the highest among monoatomic anions; Br[−] shows a ΔG of 2.02 eV, Cl[−] is 1.94 eV, and F[−] also exhibits a ΔG of 2.02 eV. Despite F[−] having a stronger electron-withdrawing capability that could potentially lead to lattice distortion and changes in electronic structure similar to polyatomic anions, the larger atomic radii of Cl[−], Br[−], and I[−] result in greater energy barriers. As for

I^- , although it has the largest atomic radius and the lowest electronegativity among the halide anions, its larger size likely causes more severe lattice distortion, significantly raising the energy barrier in the hydrogenation step of NRR, thereby impacting the efficiency.

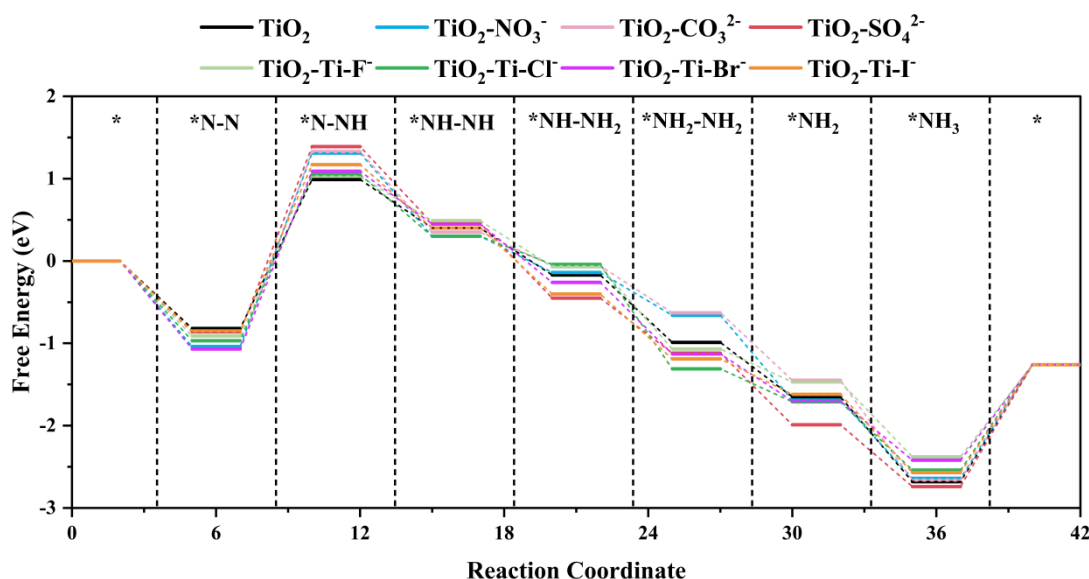
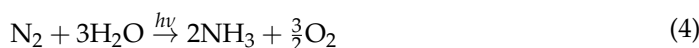


Figure 7. The Gibbs free energy for NRR on TiO_2 before and after anion adsorption. “*” represents free electrons.

In a typical photocatalytic process, the photo-induced electrons (e^-) can be transferred to the conduction band (CB) from the valence band (VB), and the holes (h^+) can be formed in the VB under visible light irradiation (Equation (1)). Subsequently, the photo-induced e^- would react with N_2 to form NH_3 directly (Equation (2)), and h^+ in VB will react with H_2O molecules to generate O_2 during the reaction (Equation (3)).



Aside from this rate-controlling step, the remaining hydrogenation processes proceed along a spontaneous downhill pathway [35]. Overall, the adsorption of various anions on TiO_2 hinders the effective activation of the $\text{N}\equiv\text{N}$ bond, thereby impeding the initiation of NRR to varying degrees. The effects of polyatomic anions are generally more pronounced, while the influence of monoatomic anions, although milder, still increases the energy barrier and weakens the catalytic activity of TiO_2 .

The individual steps of the alternating mechanism can be expressed as the following reaction equations:





The corresponding changes in Gibbs free energy (ΔG) can be calculated as follows:

$$\Delta G_1 = G(* \text{N} - \text{N}) - G(*) - G(\text{N}_2) \quad (13)$$

$$\Delta G_2 = G(* \text{N} - \text{NH}) - G(* \text{N} - \text{N}) - G(\text{H}) \quad (14)$$

$$\Delta G_3 = G(* \text{NH} - \text{NH}) - G(* \text{N} - \text{NH}) - G(\text{H}) \quad (15)$$

$$\Delta G_4 = G(* \text{NH} - \text{NH}_2) - G(* \text{NH} - \text{NH}) - G(\text{H}) \quad (16)$$

$$\Delta G_5 = G(* \text{NH}_2 - \text{NH}_2) - G(* \text{NH} - \text{NH}_2) - G(\text{H}) \quad (17)$$

$$\Delta G_6 = G(* \text{NH}_2) + G(\text{NH}_3) - G(* \text{NH}_2 - \text{NH}_2) - G(\text{H}) \quad (18)$$

$$\Delta G_7 = G(* \text{NH}_3) - G(* \text{NH}_2) - G(\text{H}) \quad (19)$$

$$\Delta G_8 = G(*) + G(\text{NH}_3) - G(* \text{NH}_3) \quad (20)$$

3. Computational Methods and Models

To study the changes in the electrical and optical properties of TiO_2 after the adsorption of anions, we employ the Vienna ab initio simulation package (VASP) to perform first-principles calculations based on density functional theory (DFT). The projected augmented wave (PAW) method employs the Perdew–Burke–Ernzerhof (PBE) generalized gradient approximation (GGA) to characterize the exchange–correlation interactions and core electrons [36]. To solve the problem of underestimation of the band gap that is observed if standard DFT methods are used, the HSE06 hybrid functional was used [37]. By including this, it allowed for a thorough analysis of the electrical characteristics, leading to a more precise representation of the band structure. To avoid spurious interactions arising from the periodic boundary conditions used in the simulations, a vacuum layer of 20 Å thickness was inserted [38]. A plane-wave basis set with an energy cutoff of 550 eV was implemented to ensure computational precision [39]. Moreover, the convergence criterion for energy was set at 10^{-5} eV and for force was set at 0.01 eV/Å so as to allow full relaxation of all geometric structures [40].

The research calculates the adsorption energies using the following formula:

$$E_{\text{ads}} = E_{\text{total}} - (E_{\text{substrate}} + E_{\text{adsorbate}})$$

The overall energy of the system with the adsorbed species is denoted as E_{total} , the energy of the clean substrate is denoted as $E_{\text{substrate}}$, and the energy of the isolated adsorbate molecule is denoted as $E_{\text{adsorbate}}$.

The calculation of the Gibbs free energy change (ΔG) for the stages of the NRR is performed using the following formula:

$$\Delta G = \Delta E + \Delta ZPE - T\Delta S$$

The reaction energy derived from DFT calculations is denoted as ΔE , the entropy contribution at 298.15 K is denoted as $T\Delta S$, and the zero-point energy difference is denoted as ΔZPE [41].

This work utilized a highly refined model of the rutile TiO_2 (001) surface, which was particularly developed to examine surface interactions and reactions. The lattice constants of the pristine rutile TiO_2 , as reported in the literature, and the relative errors from GGA calculations are summarized in Table 3 [42], demonstrating excellent agreement. The discrepancies in the a and b lattice constants are nearly 0%, while the difference along the c-axis is only 1.26%. The model was expanded to include four distinct atomic layers, comprising a total of 96 atoms, with 32 titanium (Ti) atoms and 64 oxygen (O) atoms.

Table 3. Comparison of the theoretical model and experimental measurements of the lattice constants for rutile TiO₂.

Category	Lattice Constants (Å)	
	a/b	c
This work	3.78	9.62
Experimental	3.78	9.50
Difference	0%	1.26%

4. Conclusions

This work utilized density functional theory (DFT) to examine the influence of anion adsorption on the electrical and optical characteristics of the rutile TiO₂ (001) surface. From the results of the present work, it can be concluded that typical anions inherent in water influence the photocatalytic activity of TiO₂. Indeed, the presence of anions modifies the energy gap between the valence and conduction bands, the distribution of energy levels, and the ability of light absorption. These changes directly influence the ability to inhibit charge carrier separation and recombination. Additionally, complex anions such as NO₃[−], CO₃^{2−}, and SO₄^{2−} significantly increase the energy barrier for the NRR process, thereby reducing the photocatalytic activity of TiO₂. These findings would help build and refer to a significant theoretical framework and guide to work with TiO₂ photocatalysts in multicomponent aqueous systems.

Author Contributions: X.J.: Conceptualization, Methodology, Data curation, Writing—original draft; M.G.: Validation, Formal analysis; H.L.: Writing—review and editing, Conceptualization, Methodology, Project administration, Funding acquisition. All authors have read and agreed to the published version of the manuscript.

Funding: This work was financially supported by the National Key Research and Development Program (No. 2022YFE0134600).

Institutional Review Board Statement: This study did not require ethical approval.

Informed Consent Statement: Not applicable.

Data Availability Statement: The original contributions presented in the study are included in the article material, further inquiries can be directed to the corresponding authors.

Conflicts of Interest: The authors declare no competing financial interests.

References

- Bai, W.; Shi, L.; Li, Z.; Liu, D.; Liang, Y.; Han, B.; Qi, J.; Li, Y. Recent progress on the preparation and application in photocatalysis of 2D MXene-based materials. *Mater. Today Energy* **2024**, *41*, 101547. [[CrossRef](#)]
- Aldosari, O.F.; Hussain, I. Unlocking the potential of TiO₂-based photocatalysts for green hydrogen energy through water-splitting: Recent advances, future perspectives and techno feasibility assessment. *Int. J. Hydrogen Energy* **2024**, *59*, 958–981. [[CrossRef](#)]
- Meng, D.; Ruan, X.; Xu, M.; Jiao, D.; Fang, G.; Qiu, Y.; Zhang, Y.; Zhang, H.; Ravi, S.K.; Cui, X. An S-scheme artificial photosynthetic system with H-TiO₂/g-C₃N₄ heterojunction coupled with MXene boosts solar H₂ evolution. *J. Mater. Sci. Technol.* **2025**, *211*, 22–29. [[CrossRef](#)]
- Li, Z.; Wang, S.; Wu, J.; Zhou, W. Recent progress in defective TiO₂ photocatalysts for energy and environmental applications. *Renew. Sustain. Energy Rev.* **2022**, *156*, 111980. [[CrossRef](#)]
- Imai, K.; Fukushima, T.; Kobayashi, H.; Higashimoto, S. Visible-light responsive TiO₂ for the complete photocatalytic decomposition of volatile organic compounds (VOCs) and its efficient acceleration by thermal energy. *Appl. Catal. B Environ.* **2024**, *346*, 123745. [[CrossRef](#)]
- Ren, Y.; Han, Y.; Li, Z.; Liu, X.; Zhu, S.; Liang, Y.; Yeung, K.W.K.; Wu, S. Ce and Er Co-doped TiO₂ for rapid bacteria-killing using visible light. *Bioact. Mater.* **2020**, *5*, 201–209. [[CrossRef](#)]
- Wang, H.; Hu, X.; Ma, Y.; Zhu, D.; Li, T.; Wang, J. Nitrate-group-grafting-induced assembly of rutile TiO₂ nanobundles for enhanced photocatalytic hydrogen evolution. *Chin. J. Catal.* **2020**, *41*, 95–102. [[CrossRef](#)]

8. Nakada, A.; Nishioka, S.; Vequizo, J.J.M.; Muraoka, K.; Kanazawa, T.; Yamakata, A.; Nozawa, S.; Kumagai, H.; Adachi, S.; Ishitani, O.; et al. Solar-driven Z-scheme water splitting using tantalum/nitrogen co-doped rutile titania nanorod as an oxygen evolution photocatalyst. *J. Mater. Chem. A* **2017**, *5*, 11710–11719. [[CrossRef](#)]
9. Marien, C.B.D.; Cottineau, T.; Robert, D.; Drogui, P. TiO₂ Nanotube arrays: Influence of tube length on the photocatalytic degradation of Paraquat. *Appl. Catal. B Environ.* **2016**, *194*, 1–6. [[CrossRef](#)]
10. Wang, J.; Ma, T.; Zhang, Z.; Zhang, X.; Jiang, Y.; Pan, Z.; Wen, F.; Kang, P.; Zhang, P. Investigation on the sonocatalytic degradation of methyl orange in the presence of nanometer anatase and rutile TiO₂ powders and comparison of their sonocatalytic activities. *Desalination* **2006**, *195*, 294–305. [[CrossRef](#)]
11. Xiong, Z.; Lei, Z.; Li, Y.; Dong, L.; Zhao, Y.; Zhang, J. A review on modification of facet-engineered TiO₂ for photocatalytic CO₂ reduction. *J. Photochem. Photobiol. C Photochem. Rev.* **2018**, *36*, 24–47. [[CrossRef](#)]
12. Han, Z.; Choi, C.; Hong, S.; Wu, T.-S.; Soo, Y.-L.; Jung, Y.; Qiu, J.; Sun, Z. Activated TiO₂ with tuned vacancy for efficient electrochemical nitrogen reduction. *Appl. Catal. B Environ.* **2019**, *257*, 117896. [[CrossRef](#)]
13. Padayachee, D.; Mahomed, A.S.; Singh, S.; Friedrich, H.B. Effect of the TiO₂ Anatase/Rutile Ratio and Interface for the Oxidative Activation of n-Octane. *ACS Catal.* **2020**, *10*, 2211–2220. [[CrossRef](#)]
14. Mahmood Katun, M.; Kadzutu-Sithole, R.; Moloto, N.; Nyamupangedengu, C.; Gomes, C. Improving Thermal Stability and Hydrophobicity of Rutile-TiO₂ Nanoparticles for Oil-Impregnated Paper Application. *Energies* **2021**, *14*, 7964. [[CrossRef](#)]
15. Xu, H.; Shi, J.-L.; Lyu, S.; Lang, X. Visible-light photocatalytic selective aerobic oxidation of thiols to disulfides on anatase TiO₂. *Chin. J. Catal.* **2020**, *41*, 1468–1473. [[CrossRef](#)]
16. Lai, Z.; Peng, F.; Wang, H.; Yu, H.; Zhang, S.; Zhao, H. A new insight into regulating high energy facets of rutile TiO₂. *J. Mater. Chem. A* **2013**, *1*, 4182–4185. [[CrossRef](#)]
17. Guo, Q.; Zhou, C.; Ma, Z.; Yang, X. Fundamentals of TiO₂ Photocatalysis: Concepts, Mechanisms, and Challenges. *Adv. Mater.* **2019**, *31*, e1901997. [[CrossRef](#)]
18. Guo, Q.; Ma, Z.; Zhou, C.; Ren, Z.; Yang, X. Single Molecule Photocatalysis on TiO₂ Surfaces. *Chem. Rev.* **2019**, *119*, 11020–11041. [[CrossRef](#)]
19. Low, J.; Cheng, B.; Yu, J. Surface modification and enhanced photocatalytic CO₂ reduction performance of TiO₂: A review. *Appl. Surf. Sci.* **2017**, *392*, 658–686. [[CrossRef](#)]
20. Cai, Q.; Wang, F.; He, J.; Dan, M.; Cao, Y.; Yu, S.; Zhou, Y. Oxygen defect boosted photocatalytic hydrogen evolution from hydrogen sulfide over active {0 0 1} facet in anatase TiO₂. *Appl. Surf. Sci.* **2020**, *517*, 146198. [[CrossRef](#)]
21. Pekakis, P.A.; Xekoukoulotakis, N.P.; Mantzavinos, D. Treatment of textile dyehouse wastewater by TiO₂ photocatalysis. *Water Res.* **2006**, *40*, 1276–1286. [[CrossRef](#)]
22. Saleh, R.; Taufik, A.; Prakoso, S.P. Fabrication of Ag₂O/TiO₂ composites on nanographene platelets for the removal of organic pollutants: Influence of oxidants and inorganic anions. *Appl. Surf. Sci.* **2019**, *480*, 697–708. [[CrossRef](#)]
23. Habiba, U.; Islam, M.S.; Siddique, T.A.; Afifi, A.M.; Ang, B.C. Adsorption and photocatalytic degradation of anionic dyes on Chitosan/PVA/Na-Titanate/TiO₂ composites synthesized by solution casting method. *Carbohydr. Polym.* **2016**, *149*, 317–331. [[CrossRef](#)] [[PubMed](#)]
24. Guan, D.; Xu, H.; Zhang, Q.; Huang, Y.-C.; Shi, C.; Chang, Y.-C.; Xu, X.; Tang, J.; Gu, Y.; Pao, C.-W. Identifying a Universal Activity Descriptor and a Unifying Mechanism Concept on Perovskite Oxides for Green Hydrogen Production. *Adv. Mater.* **2023**, *35*, 2305074. [[CrossRef](#)]
25. Tan, Y.; Shao, M.; Legesse, M.; Mellouhi, F.E.; Bentría, E.T.; Madjet, M.E.; Fisher, T.S.; Kais, S.; Alharbi, F.H. A Universal Chemical-Induced Tensile Strain Tuning Strategy to Boost Oxygen-Evolving Electrocatalysis on Perovskite Oxides. *Appl. Phys. Rev.* **2022**, *9*, 011422.
26. Wang, Y.; Huang, L.; Zhang, T.C.; Wang, Y.; Yuan, S. Visible-Light-Induced photocatalytic oxidation of gaseous ammonia on Mo, c-codoped TiO₂: Synthesis, performance and mechanism. *Chem. Eng. J.* **2024**, *482*, 148811. [[CrossRef](#)]
27. Ma, X.; Wu, X.; Wang, H.; Wang, Y. A Janus MoSSe monolayer: A potential wide solar-spectrum water-splitting photocatalyst with a low carrier recombination rate. *J. Mater. Chem. A* **2018**, *6*, 2295–2301. [[CrossRef](#)]
28. Huang, L.; Cui, H.; Zhang, W.; Pu, D.; Zeng, G.; Liu, Y.; Zhou, S.; Wang, C.; Zhou, J.; Wang, C.; et al. Efficient Narrow-Bandgap Mixed Tin-Lead Perovskite Solar Cells via Natural Tin Oxide Doping. *Adv. Mater.* **2023**, *35*, e2301125. [[CrossRef](#)]
29. Zhao, X.; Hu, G.; Chen, G.F.; Zhang, H.; Zhang, S.; Wang, H. Comprehensive Understanding of the Thriving Ambient Electrochemical Nitrogen Reduction Reaction. *Adv. Mater.* **2021**, *33*, e2007650. [[CrossRef](#)]
30. Trangwachirachai, K.; Kao, I.T.; Huang, W.-H.; Chen, C.-L.; Lin, Y.-C. Co-activation of methane and nitrogen to acetonitrile over MoC_x/Al₂O₃ catalysts. *Catal. Sci. Technol.* **2023**, *13*, 5248–5258. [[CrossRef](#)]
31. Zhao, R.; Wang, G.; Mao, Y.; Bao, X.; Wang, Z.; Wang, P.; Liu, Y.; Zheng, Z.; Dai, Y.; Cheng, H.; et al. Li-intercalation boosted oxygen vacancies enable efficient electrochemical nitrogen reduction on ultrathin TiO₂ nanosheets. *Chem. Eng. J.* **2022**, *430*, 133085. [[CrossRef](#)]
32. Zhang, L.; Ding, L.X.; Chen, G.F.; Yang, X.; Wang, H. Ammonia Synthesis Under Ambient Conditions: Selective Electroreduction of Dinitrogen to Ammonia on Black Phosphorus Nanosheets. *Angew. Chem. Int. Ed.* **2019**, *58*, 2612–2616. [[CrossRef](#)] [[PubMed](#)]
33. Li, H.; Gu, S.; Sun, Z.; Guo, F.; Xie, Y.; Tao, B.; He, X.; Zhang, W.; Chang, H. The in-built bionic “MoFe cofactor” in Fe-doped two-dimensional MoTe₂ nanosheets for boosting the photocatalytic nitrogen reduction performance. *J. Mater. Chem. A* **2020**, *8*, 13038–13048. [[CrossRef](#)]

34. Vedhanarayanan, B.; Chiu, C.-C.; Regner, J.; Sofer, Z.; Seetha Lakshmi, K.C.; Lin, J.-Y.; Lin, T.-W. Highly exfoliated NiPS₃ nanosheets as efficient electrocatalyst for high yield ammonia production. *Chem. Eng. J.* **2022**, *430*, 132649. [[CrossRef](#)]
35. Li, H.; Zhao, H.; Li, C.; Li, B.; Tao, B.; Gu, S.; Wang, G.; Chang, H. Redox regulation of photocatalytic nitrogen reduction reaction by gadolinium doping in two-dimensional bismuth molybdate nanosheets. *Appl. Surf. Sci.* **2022**, *600*, 154105. [[CrossRef](#)]
36. Yalcin, O.; Wachs, I.E.; Onal, I. Role of chromium in Cr–Fe oxide catalysts for high temperature water-gas shift reaction—A DFT study. *Int. J. Hydrogen Energy* **2021**, *46*, 17154–17162. [[CrossRef](#)]
37. Wang, Z.; Wang, Q.; Han, Y.; Ma, Y.; Zhao, H.; Nowak, A.; Li, J. Deep learning for ultra-fast and high precision screening of energy materials. *Energy Storage Mater.* **2021**, *39*, 45–53. [[CrossRef](#)]
38. Zhao, P.; Zheng, J.; Guo, P.; Jiang, Z.; Cao, L.; Wan, Y. Electronic and magnetic properties of Re-doped single-layer MoS₂: A DFT study. *Comput. Mater. Sci.* **2017**, *128*, 287–293. [[CrossRef](#)]
39. Pašti, I.A.; Jovanović, A.; Dobrota, A.S.; Mentus, S.V.; Johansson, B.; Skorodumova, N.V. Atomic adsorption on pristine graphene along the Periodic Table of Elements—From PBE to non-local functionals. *Appl. Surf. Sci.* **2018**, *436*, 433–440. [[CrossRef](#)]
40. Gu, X.; Luo, Y.; Li, Q.; Wang, R.; Fu, S.; Lv, X.; He, Q.; Zhang, Y.; Yan, Q.; Xu, X.; et al. First-Principle Insight Into the Effects of Oxygen Vacancies on the Electronic, Photocatalytic, and Optical Properties of Monoclinic BiVO₄(001). *Front. Chem.* **2020**, *8*, 601983. [[CrossRef](#)]
41. Guo, H.; Li, L.; Wang, X.; Yao, G.; Yu, H.; Tian, Z.; Li, B.; Chen, L. Theoretical Investigation on the Single Transition-Metal Atom-Decorated Defective MoS₂ for Electrocatalytic Ammonia Synthesis. *ACS Appl. Mater. Interfaces* **2019**, *11*, 36506–36514. [[CrossRef](#)] [[PubMed](#)]
42. Buchanan, R.C.; Park, T. *Materials Crystal Chemistry*; Marcel Dekker: New York, NY, USA, 1997.

Disclaimer/Publisher’s Note: The statements, opinions and data contained in all publications are solely those of the individual author(s) and contributor(s) and not of MDPI and/or the editor(s). MDPI and/or the editor(s) disclaim responsibility for any injury to people or property resulting from any ideas, methods, instructions or products referred to in the content.